Three-Dimensional Optical Crystals and Localized Structures in Cavity Second Harmonic Generation

M. Tlidi and Paul Mandel

Optique Nonlinéaire Théorique, Campus Plaine Code Postal 231, Université Libre de Bruxelles, 1050 Bruxelles, Belgium

(Received 27 April 1999)

By using an order parameter description of the type-II second harmonic generation, we prove analytically that different 3D periodic solutions exist and have overlapping domains of stability. The stable periodic solutions are lamellae, 3D hexagons, and a body-centered cubic pattern. The coexistence of periodic and homogeneous solutions leads to localized structures such as light drops and cylinders which are found numerically.

PACS numbers: 42.65.Sf, 42.60.Mi, 42.65.Pc

Pattern formation is an important and active topic in nonlinear optics. Early theoretical approaches have predicted the occurrence of spatial patterns in the transverse intracavity field due to the interplay between Kerr media and diffraction [1,2]. Since then, various types of periodic or localized patterns have been observed in optical devices. This topic has been abundantly discussed and is by now fairly understood (see Refs. [3,4] for reviews).

In another line of research, theoretical and experimental studies have shown that the chromatic dispersion, due to the intracavity medium, plays an important role in the dynamics of nonlinear optical systems, and may induce a temporal modulational instability [5,6]. In the theoretical studies, diffraction is neglected, e.g., the intracavity fields are spatially stabilized by using guided-wave structures. For a coherently driven passive ring cavity with a Kerr medium, a purely analytic study indicates that the chromatic dispersion may destabilize the hexagonal patterns and allows the formation of three-dimensional (3D) body centered cubic (bcc) structures in the cavity field [7]. These structures consist of regular 3D lattices of bright spots traveling at the group velocity of light in the material. They dominate the nonlinear dynamics of the dispersive and diffractive Kerr nonlinearity near the modulational instability.

The purpose of this Letter is to report on analytic and numerical investigations of 3D periodic patterns due to the combined influence of diffraction and chromatic dispersion in intracavity type-II second harmonic generation (SHG). This process involves the field polarization degrees of freedom due to the birefringence of the $\chi^{(2)}$ crystal.

Close to the modulational threshold where patterns emerge, we derive a Swift-Hohenberg (SH) equation with real coefficients and both quadratic and cubic nonlinearities. As a result, we are able to prove analytically that the bcc, 3D hexagonal and lamella patterns have overlapping finite domains of stability, while the rhombic and face-centered cubic (fcc) lattices are completely unstable. These results are supported by numerical simulations. Similar structures have been observed in chemical systems [8], and in lasers [9]. In a very general context, Pismen has recently studied the role of 3D topological defects in nonequilibrium systems [10].

More importantly, in the regime where the stable homogeneous steady state (HSS) coexists with the 3D periodic crystals, an additional variety of stable 3D localized structures (LS) can be generated. They result in the confinement of the intracavity field both in space and time, leading to isolated light drops and cylinders. The existence of these 3D LS does not require a bistable HSS. They can be stable in the regime where the single HSS exhibits a subcritical modulational instability.

The optical system we consider is the type-II SHG: an optical cavity filled with a $\chi^{(2)}$ medium and coherently driven by an injected signal at frequency ω produces a field at 2ω. We assume the validity of the mean field approximation (high finesse cavity) which oscillates on only one longitudinal mode. Taking into account diffraction and chromatic dispersion, type-II SHG can be described by the following dimensionless partial differential equations:

$$\frac{\partial E_0}{\partial t} = -(1 + i\Delta_0)E_0 - E_1E_2 + d_0\frac{\partial E_0}{\partial \tilde{\tau}} + i\left(\mathcal{L}_\perp + \frac{\partial^2}{\partial \tilde{\tau}^2}\right)E_0, \tag{1}$$

$$\frac{1}{\gamma}\frac{\partial E_1}{\partial t} = -(1 + i\Delta_1)E_1 + E_0E_2^\star + E\cos\theta + d_1\frac{\partial E_1}{\partial \tilde{\tau}} + i\left(\alpha\mathcal{L}_\perp + \delta\frac{\partial^2}{\partial \tilde{\tau}^2}\right)E_1, \tag{2}$$

$$\frac{1}{\gamma}\frac{\partial E_2}{\partial t} = -(1 + i\Delta_2)E_2 + E_0E_1^\star + E\sin\theta + d_2\frac{\partial E_2}{\partial \tilde{\tau}} + i\left(\alpha\mathcal{L}_\perp + \delta\frac{\partial^2}{\partial \tilde{\tau}^2}\right)E_2, \tag{3}$$

where $E_{1,2}$ are the normalized slowly varying envelopes of the fundamental fields at frequency ω, polarized along the $\tilde{x}$ and $\tilde{y}$ orthogonal transverse directions. E_0 is the second harmonic envelope at frequency 2ω. The time t, describing the slow evolution of the field envelopes between two consecutive cavity round-trips, has been scaled such that

the decay rate of the second harmonic is unity. $\tilde{\tau}$ is the time in a reference frame traveling at the group velocity of light in the $\chi^{(2)}$ medium. γ is the ratio of the photon lifetimes at frequencies 2ω and ω. The input field E is linearly polarized in a direction forming an angle θ with the transverse $\tilde{y}$ axis. $\mathcal{L}_\perp = \partial^2/\partial\tilde{x}^2 + \partial^2/\partial\tilde{y}^2$ is the Laplace operator in the transverse plane $(\tilde{x}, \tilde{y})$. The parameters d_j represent the group velocity of the fields E_j. The phase matching condition imposes that the ratio of the diffraction coefficients be $\alpha = 2$ [11]. $\delta = \beta_1/\beta_2$, where $\beta_{1,2}$ are the dispersion coefficients at frequency ω and 2ω, respectively. δ can be positive or negative, depending on the relative position of the zero material dispersion with respect to ω and 2ω. We analyze the anomalous dispersion regime for which $\delta > 0$. In that case, the second-order derivatives form a 3D Laplace operator acting in the Euclidean space (x, y, τ), with $x = \tilde{x}/\sqrt{\alpha}$, $y = \tilde{y}/\sqrt{\alpha}$ and $\tau = \tilde{\tau}/\sqrt{\delta}$.

We focus our analysis on the situation usually realized experimentally, namely, quasisymmetric pumping ($\theta \approx 45°$). With this simplification, it is more convenient to introduce the following decomposition of the fundamental fields, the detuning and the injected signal: $E_\pm = (E_1 \pm E_2)/\sqrt{2}$, $\Delta_\pm = (\Delta_1 \pm \Delta_2)/\sqrt{2}$, and $Y_\pm = E(\cos\theta \pm \sin\theta)\sqrt{2}$. It has been demonstrated recently by Longhi [12] that, in the limit Δ_0, $\Delta_+ \sim \mathcal{O}(\varepsilon)$, $\Delta_- \sim \mathcal{O}(\varepsilon^2)$, $E_+ \sim \mathcal{O}(\varepsilon^2)$, $E_- \sim \mathcal{O}(\varepsilon^3)$, $d_0, d_1 \sim \mathcal{O}(\varepsilon)$, and $d_2 \sim \mathcal{O}(\varepsilon^2)$ where ε is a small parameter, the two–dimensional (2D) spatiotemporal dynamics of type-II SHG can be described by an SH equation. Taking into account chromatic dispersion and fixing $\gamma = 1$ for simplicity, a similar multiple-time scale expansion leads to the generalization of the SH equation derived for type-II SHG

$$\frac{\partial X}{\partial t} = S + X\left(\mu - \frac{\sqrt{2}}{8}X^2\right) + \Delta_+ \mathcal{L}\, X - \frac{1}{2}\mathcal{L}^2 X\,. \tag{4}$$

In this equation, $E_- = (1 - i\Delta_-)X + i\mathcal{L}X$ so that $X = \mathrm{Re}(E_-)$, $\mathcal{L} \equiv \partial^2/\partial x^2 + \partial^2/\partial y^2 + \partial^2/\partial\tau^2$, $S = \Delta_-(\Delta_0 - \Delta_+)\sqrt{2} + Y_-$, and $\mu = \sqrt{2}[-3(\Delta_+ - \Delta_0)^2 + 4\Delta_0^2 + 2\sqrt{2}\,Y_+ - 8]/16$. The homogeneous steady states of Eq. (4) are the solutions of $S + \mu X_s - \sqrt{2}\,X_s^3/8 = 0$. There is bistability if $\mu > 0$. A linear stability shows that the HSSs undergo a modulational instability leading to periodic patterns. This instability occurs in the range $S_{M-} < S < S_{M+}$, where $S_{M\pm} = \pm(\Delta_+^2 - 2\mu)X_{M\pm}/3$ and $X_{M\pm} = \pm 2\sqrt{\sqrt{2}(\Delta_+^2 + \mu)/3}$. In this interval, there exists a finite band of Fourier modes q_j which are linearly unstable and trigger spontaneously the evolution of the intracavity field toward the formation of regular lattices of 3D bright spots (or light bullet [13,14]) traveling at the group velocity of the light within the cavity. This instability is caused by the competition between two processes: (i) diffraction and chromatic dispersion which tend to restore both spatial and temporal uniformity in the (x, y, τ) space, and (ii) the nonlinearity that is responsible for the amplification of both spatial and temporal inhomogeneities. The balance between the two processes generates well-known spatial and temporal modulational instabilities. The maximum gain (i.e., the most unstable wave number) is $q_M = \sqrt{-\Delta_+}$. It is the same at both bifurcation points. In between, the HSS solution is linearly unstable with respect to fluctuations with wave vectors $\mathbf{q_j}$ having the same maximum wave number $q = q_M$ but arbitrary direction in the 3D Fourier space. Since the system is isotropic in the (x, y, τ) space, these unstable wave vectors do not have any preferred direction. Although an indefinite number of modes may be generated with arbitrary directions, a regular pattern is selected and emerges due to the nonlinear interaction. Our purpose here is to study analytically this 3D pattern selection mechanism in the weakly nonlinear regime where the HSS is monostable ($\mu < 0$). For this purpose, we introduce the deviation $u(x, y, \tau, t)$ from the HSS as $X(x, y, \tau, t) = X_s + u(x, y, \tau, t)$. There is no assumption yet that these deviations are small. Under this transformation, Eq. (4) becomes

$$\frac{\partial u}{\partial t} = \left(\mu - \frac{3\sqrt{2}}{8}X_s^2\right)u - \frac{3\sqrt{2}}{8}X_s u^2 - \frac{\sqrt{2}}{8}u^3 + \Delta_+ \mathcal{L}\, u - \frac{1}{2}\mathcal{L}^2 u\,. \tag{5}$$

To calculate the solutions emerging from the modulational critical points, we use the weakly nonlinear theory to derive amplitude equations for the critical modes and assess their stability. To this end, we introduce a small parameter η which measures the distance from the modulational instability: $|(S - S_{M\pm})/S_{M\pm}| = \eta$. Let us focus on the instability around (S_{M-}, X_{M-}). The analysis of the 3D structures around (S_{M+}, X_{M+}) is the same since Eq. (4) is invariant under the inversion symmetry $(S, X) \to (-S, -X)$. Next, we expand the variable $u(x, y, \tau, t)$, the parameter S, and X_s in powers of η: $(S, X_s, u) = (S_{M-}, X_{M-}, 0) + \sum_i \eta^i (s_i, a_i, u_i)$. To leading order in η, the solution of Eq. (5) is a linear superposition of ℓ pairs of opposite wave vectors $\mathbf{q_j}$ lying on the critical sphere of radius q_M:

$$u_0 = \sum_{j=1}^{\ell} [W_j \exp i(\mathbf{q_j}.\mathbf{r}) + \text{c.c.}], \qquad |\mathbf{q_j}| = q_M = \sqrt{-\Delta_+}\,, \tag{6}$$

where c.c. denotes the complex conjugate. The stripes (or lamellae) and rhombic cells are characterized by $\ell = 1$ and $\ell = 2$, respectively, and the 3D hexagons (or hexagonally packed cylinders) are obtained for $\ell = 3$ with $\mathbf{q_1} + \mathbf{q_2} + \mathbf{q_3} = \mathbf{0}$ and $q_j = q_M$. The face-centered cubic (fcc) lattice and the quasiperiodic crystals correspond to $\ell = 4$ and $\ell = 5$, respectively. The body-centered cubic (bcc) lattice is obtained for $\ell = 6$. Since we are interested in the analysis of the 3D structures with periodic boundary conditions, quasiperiodic crystals ($\ell = 5$) are not considered.

The 3D structures corresponding to $\ell = 2$ (rhombic lattice) and $\ell = 4$ (fcc lattice) are always less stable than the lamellae, the hexagons, and the bcc structures. In the following, we will therefore consider only the formation and the competition between these three classes of structures.

Following the approach used in [7], we derived a set of mode amplitude equations for the different 3D structures. The linear stability analysis of these structures against internal perturbations of their steady-state solutions and the relative stability analysis, i.e., the stability of one pattern against perturbations favoring another structure, indicate the occurrence of transitions and multistability between these 3D structures. The results of that stability analysis are summarized in the bifurcation diagram displayed in Fig. 1, where we have plotted the maximum amplitude of lamellae, hexagons, and bcc structures versus κ, which κ is the relative distance from criticality, i.e., $\kappa = (S - S_{M\pm})/|S_{M\pm}|$. When increasing the control parameter κ from the region $\kappa < \kappa_A$, bcc structures appear first. They are stable for $\kappa_A < \kappa < \kappa_3$. The 3D hexagons are stable for $\kappa_B < \kappa < \kappa_2$. Finally, for $\kappa > \kappa_1$, lamellae are stable. Our weakly nonlinear analysis is restricted to the regime where the homogeneous steady state exhibits a supercritical modulational bifurcation, i.e., $\mu < -76/(29\Delta_+^2)$.

The predictions of the above weakly nonlinear analysis are well reproduced by numerical simulations of the dynamical equation (4). The simulations are performed with $\Delta_+ = -0.1$ and $\mu = -0.004$. For these parameters, the steady-state response curve is monostable and the modulational instability occurs at $S_{M-} \approx -1.88 \times 10^{-4}$. We have used two numerical codes, one based on the Euler explicit scheme and the other on a pure implicit scheme, supplemented by finite difference methods [15]. The two numerical methods give the same results. The 3D solutions presented here are obtained by using periodic boundary conditions in the three directions. Our results are illustrated in Fig. 2, where we see that, as predicted by the weakly nonlinear analysis, the sequence bcc–3D hexagons–lamellae are observed. Note, however, that for the parameters we have chosen the lamellae have already undergone a zigzag instability.

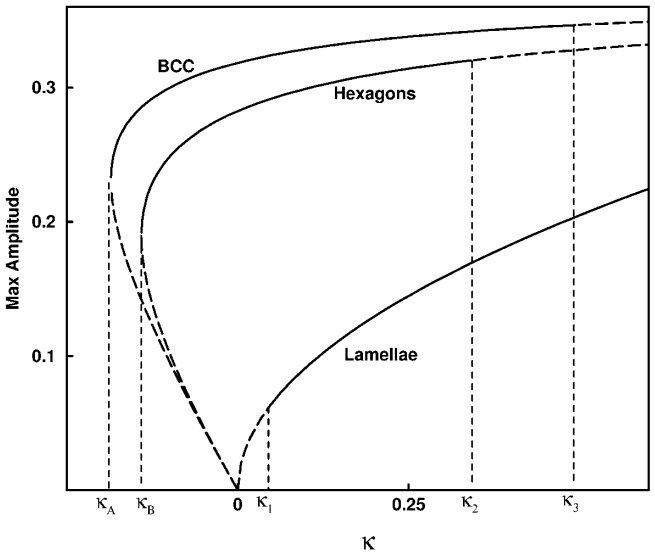

FIG. 1. 3D bifurcation diagram obtained from the weakly nonlinear analysis. The solid and the dashed lines correspond, respectively, to stable and unstable solutions. Parameters are $\Delta_+ = -0.1$ and $\mu = -0.004$.

Once the periodic solutions of Eq. (4) are characterized, it is natural to seek 3D localized solutions of the type discussed in [16,17] in the transverse plane, and experimentally observed in [18]. These 2D localized structures have been recently obtained in the intracavity second harmonic generation of both type-I and type-II [12,19]. In the present problem, the 3D localized structures will be spheres in the 3D space (x, y, τ), but will be ellipsoids in the space $(\tilde{x}, \tilde{y}, \tilde{\tau})$. They are homoclinic or multisolitonic solutions connecting the homogeneous and periodic solutions in the domain where they coexist as stable solutions. The homoclinic nature of these solutions implies that for a given set of control parameters, the number and the space-time distribution of 3D LS immersed in the bulk of the basic HSS are determined by the initial condition: there exist a large number of 3D LS, and the system selects one of them on the basis of the initial condition. As an example, an initial transverse profile which presents a pointlike peak

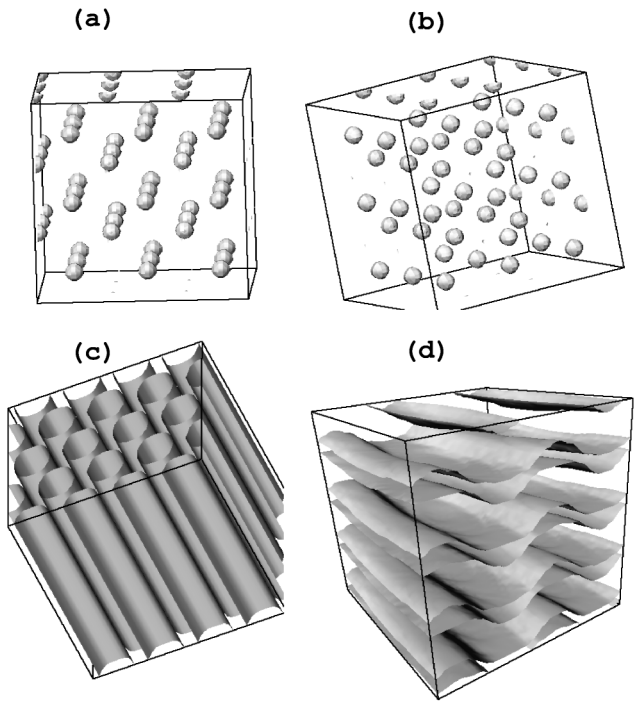

FIG. 2. Isosurface of $X = \mathrm{Re}(E_-)$ corresponding to the 3D periodic solutions of Eq. (4) obtained from numerical simulations. Mesh number integration is $50 \times 50 \times 50$. (a),(b) The same bcc pattern ($S = -2.0 \times 10^{-4}$) viewed from two different angles. (c) 3D hexagons with $S = -1.5 \times 10^{-4}$. (d) Lamellae with $S = -1.0 \times 10^{-4}$.

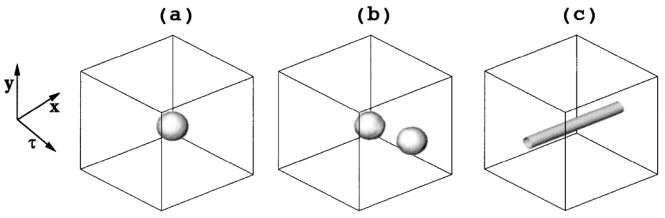

FIG. 3. Isosurface of $X = \mathrm{Re}(E_-)$ corresponding to the 3D localized solutions of Eq. (4) obtained from numerical simulations. (a) Localized light drop for $\Delta_+ = -0.2$ and $\mu = -0.01$ and $S = -2.3 \times 10^{-3}$. (b) Two localized light drops for the same parameters as in (a) but a different initial condition. (c) Localized cylinder for $\Delta_+ = -0.025$, $\mu = 0.1$, and $S = 1.5 \times 10^{-4}$. Mesh number integration is $50 \times 50 \times 50$.

evolves toward a single light drop (see Fig. 3a). This space and time confinement of the light is specific to the domain where the system exhibits bistability between the bcc crystal and the HSS below the instability threshold S_{M-}. The maximum intensity in the center of this light drop is essentially the same as in the corresponding bcc crystal and the width is approximatly half the critical wavelength given by the linear stability analysis. This confinement of the intracavity field can be interpreted as a 3D front (or switching wave) which undergoes a self-trapping (pinning effect) between the bcc crystal and HSS which are both stable.

If initially the distance between two pointlike peak profiles in the transverse plane is larger than the critical wavelength, these two perturbations evolve independently and the final 3D LS consist of two localized light drops (see Fig. 3b). Similarly, a single cylinder can be also generated in the regime where the hexagonal crystal coexists with the stable HSS (see Fig. 3c). Metastable tori have also been observed: starting with a circle as the initial condition, a torus emerges and persists for an unusually long time (up to $t \approx 750$), before breaking into a cloud of localized drop.

Localized structures may therefore be useful for signal processing since the addition or removal of a localized sphere simply means the change from one solution to another solution of Eq. (4).

It is clear that the domain of validity of the results presented in this Letter is limited by the scaling introduced to derive the SH equation [Eq. (4)]. In 2D, it has been shown that beyond this domain of parameters, new instabilities appear, which modify the bifurcation sequences [20,21]. The same effect is expected if the present analysis is generalized to the complete set of Eqs. (1)–(3).

We acknowledge fruitful discussions with R. Lefever, M. Haelterman and M. Le Berre. This work was supported by the Fonds National de la Recherche Scientifique and the Interuniversity Attraction Pole program of the Belgian government.

[1] L. A. Lugiato and R. Lefever, Phys. Rev. Lett. **58**, 2209 (1987).
[2] G. Grynberg, Opt. Commun. **66**, 321 (1988).
[3] N. N. Rosanov, *Progress in Optics* (North-Holland, Amsterdam, 1996), Vol. XXXV; P. Mandel, *Theoretical Problems in Cavity Nonlinear Optics* (Cambridge University Press, Cambridge, England, 1997); L. A. Lugiato *et al.*, in *Advances in Atomic, Molecular and Optical Physics,* edited by B. Bedersen and H. Walther (Academic Press, New York, 1998).
[4] Special issue of Quantum Semiclass. Opt. **10**, 775–878 (1998), edited by G. de Valcárcel, E. Roldán, and R. Vilaseca; J. Opt. B: Quantum Semiclass. Opt. **1**, 1–197 (1999).
[5] M. Haelterman, S. Trillo, and S. Wabnitz, Opt. Lett. **17**, 745 (1992); Opt. Commun. **91**, 321 (1988).
[6] G. Steinmeyer, A. Schwache, and F. Mitschke, Phys. Rev. E **53**, 5399 (1996); S. Coen and M. Haelterman, Phys. Rev. Lett. **79**, 4139 (1997).
[7] M. Tlidi, M. Haelterman, and P. Mandel, Europhys. Lett. **42**, 505 (1998); Quantum Semiclass. Opt. **10**, 869 (1998).
[8] V. Castets, E. Dulos, J. Boissonade, and P. De Kepper, Phys. Rev. Lett. **64**, 2953 (1990).
[9] N. L. Komarova, B. A. Malomed, J. V. Moloney, and A. C. Newell, Phys. Rev. A **56**, 803 (1997).
[10] L. M. Pismen, Phys. Rev. E **50**, 4896 (1994); L. M. Pismen, *Vortices in Nonlinear Fields* (Oxford University Press, New York, 1998).
[11] A. Yariv and P. Yeh, *Optical Waves in Crystals* (Wiley, New York, 1984).
[12] S. Longhi, Opt. Lett. **23**, 346 (1998).
[13] Y. Sibelberg, Opt. Lett. **15**, 1282 (1990).
[14] B. A. Malomed, P. Drummond, H. He, A. Berntson, D. Anderson, and M. Lisak, Phys. Rev. E **56**, 4725 (1997).
[15] M. Tlidi, M. Georgiou, and P. Mandel, Phys. Rev. A **48**, 4605 (1993).
[16] N. N. Rosanov, Proc. SPIE Int. Soc. Opt. Eng. **1840**, 130 (1992).
[17] M. Tlidi, P. Mandel, and R. Lefever, Phys. Rev. Lett. **73**, 640 (1994); L. Yu. Glebsky and L. M. Lerman, Int. J. Nonlinear Sci. **5**, 424 (1995).
[18] W. B. Taranenko, K. Staliunas, and C. O. Weiss, Phys. Rev. A **56**, 1582 (1997).
[19] C. Etrich, U. Peschel, and F. Lederer, Phys. Rev. Lett. **79**, 2454 (1997).
[20] C. Etrich, D. Michaelis, U. Peschel, and F. Lederer, Phys. Rev. E **58**, 4005 (1998).
[21] S. Longhi, Phys. Rev. E **59**, R24 (1999); S. Longhi, Phys. Rev. A **59**, 4021 (1999).